EurJIC
European Journal of Inorganic Chemistry

Chemistry Europe
European Chemical Societies Publishing

Accepted Article

Title: EPR, Magnetic, and Computational Characterization of Linear and Zigzag Ladder-type Chains of Exchange Coupled Cu(II) Complexes with Picolinic and Dipicolinic Acid Ligands

Authors: Ana L. Pérez, Axel Kemmerer, Ricardo Baggio, Carlos A. Ramos, Sergio D. Dalosto, Mario C. G. Passeggi, Alberto C. Rizzi, and Carlos D. Brondino

To be cited as: *Eur. J. Inorg. Chem.* 10.1002/ejic.202100470

Link to VoR: https://doi.org/10.1002/ejic.202100470

WILEY-VCH

EPR, Magnetic, and Computational Characterization of Linear and Zigzag Ladder-type Chains of Exchange Coupled Cu(II) Complexes with Picolinic and Dipicolinic Acid Ligands

Dr. Ana L. Pérez,[a] Axel Kemmerer,[a] Dr. Ricardo Baggio,[b] Prof. Dr. Carlos A. Ramos,[c] Prof. Dr. Sergio D. Dalosto,[d] Prof. Dr. Mario C. G. Passeggi,[d] Prof. Dr. Alberto C. Rizzi,[a] and Prof. Dr. Carlos D. Brondino*[a]

[a] Departamento de Física, Facultad de Bioquímica y Ciencias Biológicas, Universidad Nacional del Litoral - CONICET, Ciudad Universitaria, S3000ZAA Santa Fe, Argentina

[b] Gerencia de Investigación y Aplicaciones, Centro Atómico Constituyentes, Comisión Nacional de Energía Atómica, Buenos Aires, Argentina

[c] Centro Atómico Bariloche, Comisión Nacional de Energía Atómica, Av. Bustillo 9500, 8400 Bariloche, Río Negro, Argentina

[d] Instituto de Física del Litoral, Universidad Nacional del Litoral - CONICET, Güemes 3450, 3000 Santa Fe, Argentina

*E-mail: brondino@fbcb.unl.edu.ar
Tel: + 54 342 4575213
www.fbcb.unl.edu.ar/dfbioq

Supporting information for this article is given via a link at the end of the document.

Abstract: We report magnetic, EPR, and computational studies on two representative examples of structurally well-characterized one dimension (1D) molecular systems: the copper complexes catena-[bis(μ-pyridine-2-carboxylato)-copper dihydrate] and catena-[(μ_2-pyridine-2,6-dicarboxylato)-diaqua-copper(II)], hereafter **1** and **2**, respectively. Experimental and theoretical results confirmed that the structural chains in both compounds behave as magnetic chains in which the copper ions are weakly coupled by isotropic exchange. Magnetic susceptibility measurements of **1** suggested that the copper ions are antiferromagnetically coupled whereas EPR measurements suggested ferromagnetic coupling at temperature above 100 K which becomes antiferromagnetic at low temperatures. Computational calculations would indicate that the ferromagnetic-antiferromagnetic change may be due to $d_{Cu\text{-}Oap}$ shortening on lowering temperature temperature (a fact that was observed experimentally by XRD at low temperatures), which redistributes the small Cu(II) unpaired spin density delocalized on the apical ligand to copper. The 1D magnetic behavior of the zigzag ladder chain of **2** is less detectable than that of the single chain of **1**. Magnetic susceptibility measurements in conjunction with computational calculations showed that the pathways that give rise to the 1D ladder transmit ferromagnetic exchange interactions with different strengths, with the stronger interaction being transmitted along the rungs. The role of the weaker exchange interactions transmitted along the rails on the magnetic dimensionality of **2** is analyzed.

Introduction

The study of exchange coupled systems is a field of the molecular magnetism that impacts on very different disciplines, such as the design of magnetic materials and the characterization of electron transfer pathways in redox proteins.[1] The design of solid state molecular magnets requires to synthetize compounds formed by isolated magnetic clusters, a goal difficult to achieve as the pathways that link up these centers usually transmit non-negligible exchange interactions that may shape the overall magnetic behavior of a given compound. Identical considerations apply for one dimension (1D) and two dimension (2D) magnetic systems, for which the presence of negligible inter-chain/layer exchange interactions is required [1b, 2] The impact on biology is perhaps less visualized. Biological systems such as electron transfer proteins and redox enzymes perform electron transfer reactions through long distances mediated by chemical pathways that involve paramagnetic centers bridged by non-covalent and covalent links,[3] which additionally may transmit very weak exchange interactions.[1a, 4] Exchange coupling constants associated with these links can be used to infer on the ability of these pathways to serve as electron conduits, and thus to learn on electron transfer processes in biological redox systems.[5]

In the last years, considerable efforts have been oriented to characterize 1D molecular systems coupled by exchange. Besides the theoretical interest in the study of 1D magnetic systems formed by similar and dissimilar spin topologies, the discovery that they may experiment the blocking of the magnetization at very low temperatures suggested their potential use in magnetism-based technological applications.[1b, 6] The magnetic characterization of 1D exchange coupled systems is usually performed by conventional magnetic measurements in the temperature range of 2 K-room temperature assigning the 1D magnetic axis to that predicted by structural data.[6e, 7] This methodology has proven to be very valuable, but its utility is rather limited for those cases of very weakly exchange coupled systems ($|J| < 2$ cm^{-1}), as magnetic data of extended systems in the 2 K-room temperature range show in most cases simple Curie-Weiss behaviors. These limitations can be overcome by means of single crystal EPR spectroscopy, which, irrespective of the strength of the exchange interaction, allows one to confirm unambiguously the magnetic chain direction from the angular variation of the EPR linewidth on the basis of the effect caused

by dimensionality in the spin dynamics of the systems.[8] Furthermore, these procedures have also shown in some cases not only a mismatch between magnetic and structural axes,[9] but also a different dimensionality.[10]

In addition to exchange-coupled spins along a single chain, a variety of 1D structural systems with different spin topologies have been reported.[6e, 6f, 11] Among them, ladder-type systems with parallel and zigzag rungs have been studied due to their interesting and variable quantum properties. These undoubtedly are 1D systems from a structural point of view, but, the associated spin dynamic might be different to that observed in 1D magnetic systems of single chains, as is governed by both rung and rail exchange interactions.[12]

The copper complexes catena-[bis(μ-pyridine-2-carboxylato)-copper dihydrate][13] and catena-[(μ_2-pyridine-2,6-dicarboxylato)-diaqua-copper(II)][14] (hereafter **1** and **2**, respectively) are two representative examples of structurally well-characterized 1D molecular systems. Pyridine-2-carboxylic acid and Pyridine-2,6-dicarboxylic acid, also known as Picolinic and Dipicolinic acids, respectively, are organic molecules widely studied as ligands in coordination chemistry due to their low toxicity, amphophilic nature, and numerous biological activities and immune responses.[15] The carboxylate O-atoms of Picolinic acid molecules bridge copper(II) ions yielding structural linear chains in **1**. Magnetic susceptibility measurements revealed a Curie-Weiss behavior typical of very weakly exchange coupled systems, but showed an unexpected ferromagnetic→antiferromagnetic transition on cooling.[13j] The ferromagnetic (FM) behavior observed at high temperatures is expected from the structural characteristic of **1**, but there is not a priori an apparent justification explaining the transition to an antiferromagnetic (AFM) state at low temperatures. The structure of **2** constitutes an archetype of a ladder with zigzag coupling,[14] in which the copper centers should be very weakly ferromagnetically coupled by intra- and inter-rail exchange interactions on the basis of well-established magneto-structural correlations.[16] Magnetic characterization of **2** has not been reported to the best of our knowledge.

In order to provide insight into the magnetic properties of structurally 1D systems weakly coupled by exchange, we report here a detailed study of the magnetic properties of **1** and **2**. Single crystal EPR measurements are used to unveil the magnetic dimensionality of both compounds. The causes at molecular level of the FM/AFM transition of **1** as well as the magnetic dimensionality of both compounds are also analyzed and rationalized using DFT theory.

Results and Discussion

Crystal and Molecular Structure

X-ray powder diffraction measurements performed on the bulk of the crystalized material confirmed that the synthetized compounds correspond to structures previously reported for **1** and **2** (Figure S1), but the difractogram of **1** revealed the presence of either a contamination or an extra phase. Since the purity of the samples is essential for the studies we report here, we confirmed by X-ray single crystal crystallography that the structure of **1** corresponds to those previously reported [13], and that the single crystals do not show evidences of extra phases (Table S1 contains the most important crystallographic data for **1**, together with a comparison with the structures reported by other authors which were used in the theoretical calculations. The cif file of **1** obtained by us is available upon request). The structure of **1** was firstly reported by Takenaka et al,[13r] followed by a number of reports of the same structure with variable quality.[13a-q, 13s-x] The structure of **2** was reported four times.[14] A brief description of the crystal and molecular structures of **1** and **2** as reported in [13s] and [14b] is presented in order to interpret magnetic and EPR experiments and computational calculations.

1 crystallizes in the triclinic system, space group $P\bar{1}$, Z= 1.[13s] The Cu(II) ions are in a slightly distorted octahedral environment coordinated to four carboxylic oxygen atoms (O1, O1A, O2 and O2A) and to two pyridine nitrogen atoms (N1 and N1A).

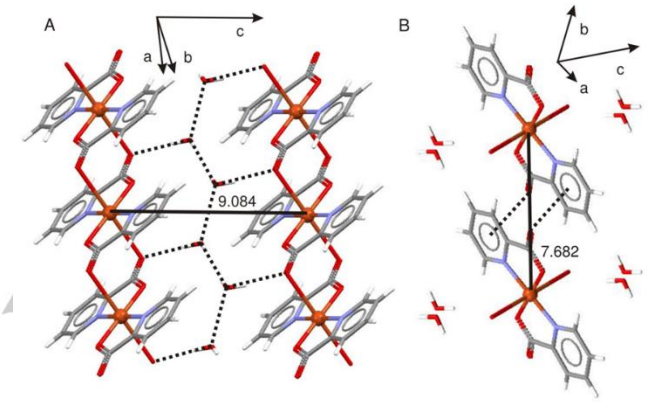

Figure 1. Coordination around the copper(II) ion of **1** and intra an inter-chain pathways linking copper(II) ions. Interchain links are provided by hydrogen bonds (A) and CO-π (B) interactions. Cu-Cu distances are in Å. Crystallographic axes are indicated.

The crystal lattice of **1** is composed of magnetically equivalent Cu(II) ion chains running along the crystallographic *a* crystal axis (Figure 1A). The intrachain pathway is composed of two symmetry related carboxylate moieties, in which the oxygen atoms act as equatorial and apical ligands to adjacent Cu(II) ions, respectively. Adjacent chains are mainly stabilized by two types of interactions. One of them is established by reticular zigzag chains, also running along the *a* crystal axis, of hydrogen-bonded water molecules (Figure 1A). The second interaction is determined by symmetrical double CO-π interactions between the carboxylate group and the picoline pyridine ring (Figure 1B). There are 24 reported crystallographic structures of **1** in the Cambridge Crystallographic Data Center.[13] Most of them were determined at room temperature whereas the remaining ones in the temperature range 99-180 K. An inspection of the cell parameters for 22 of these structures as a function of temperature reveals a slight but non-negligible distortion of the crystal unit cell when temperature varies. As temperature decreases, the lengths of the unit cell edges (*a*, *b*, *c*) and the unit cell volume decrease, whereas the angles between edges (*α*, *β*, *γ*) increase (Figure S2). Changes in unit cell parameters correlate with an expected low temperature shortening of both the Cu-O_{ap} distance and the separation between picolinic acid moieties interacting through CO-π interactions (Figure S2). This behavior will be taken into account when analyzing EPR and magnetic susceptibility results given below.

2 crystallizes in the monoclinic system, space group $P2_1/c$, Z= 4.[14b] Cu(II) ions are in a slightly distorted octahedral environment coordinated to two water oxygen atoms (O5 and O6), two carboxylic oxygen atoms (O1 and O3) and the pyridine nitrogen atom (N1) of the same Dipicolinic acid moiety, and one oxygen atom (O3C) from an adjacent Dipicolinic acid molecule. O3C and O6 occupy the apical positions of the octahedron.

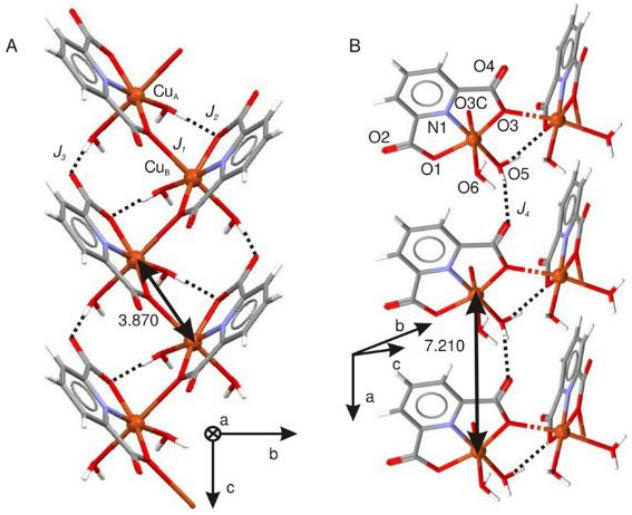

Figure 2. Coordination around copper(II) ions of **2.** A) Crystal lattice perspective showing a chain of Cu(II) ions running along the *c* crystal axis. J_1, J_2 and J_3 indicate intrachain pathways connecting Cu(II) ions. B) Crystal lattice perspective showing interchain interactions. Cu-Cu distances are in Å. Crystallographic axes are indicated.

Copper ion chains of **2** present a ladder-like structure with rails running along the *c* crystal axis and zigzag rungs (Figure 2A). The chain is composed of C2*b* symmetry related complexes identified as Cu_A (x, y, z) and Cu_B (-x, 1/2+y, 1/2-z) ($d_{Cu\text{-}Cu}$= 3.870 Å). Inter-rail pathways are identified as J_1 (–Cu–O_3–Cu–) and J_2 (–Cu–O_5…O_1–Cu–), whereas the intra-rail pathway as J_3 (–Cu–O_6…O_2–C–O_1–Cu–). Adjacent chains are stabilized by the pathway identified as J_4 in Figure 2B.

Magnetic Susceptibility Measurements

Temperature–dependent magnetic susceptibility (χ) measurements of powder samples of **1** and **2** (see experimental section for powder sample preparation) are shown in the upper and lower panels, respectively, of Figure 3 and Figure S3. Both compounds show a Curie-Weiss behavior typical of mononuclear copper(II) centers weakly coupled by exchange. A plot of χT vs T of **1** shows an antiferromagnetic behavior at low temperatures in line with Luo et al,[13j] but the χT data at high temperature do not show the constant behavior expected for weakly exchange coupled S=1/2 spins.[16] In this regard, our results are not conclusive on the ferromagnetic behavior above 40 K previously reported.[13j] On the other hand, from the comparison of all the reported structures we noted that **1** experiences subtle structural changes with temperature (Figure S2), suggesting that they could be responsible for the untypical magnetic behavior of **1** with temperature. The fact that no clear conclusion could be obtained from magnetic measurements led us to perform further EPR studies as a function of temperature for **1**, which will be shown and rationalized with DFT calculations below.

In contrast to that observed in **1**, the plot χT vs T of **2** indicates ferromagnetic coupling between copper ions in the temperature range (Figure 3, lower panel). The analysis of these data assuming a Curie-Weiss model yielded C = 0.3484 (2) emuK/mol and θ = 1.22 (3) K.

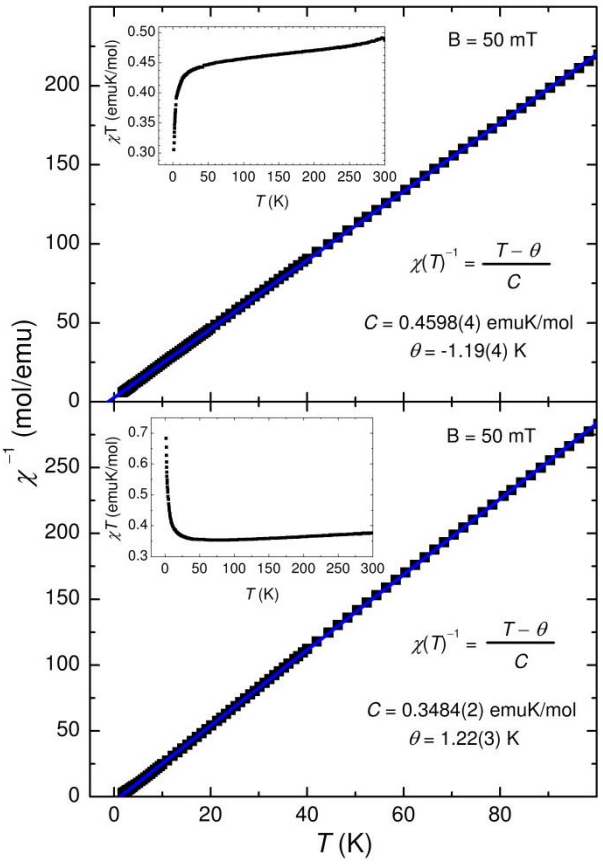

Figure 3. Plot of the inverse of the magnetic susceptibility $\chi^{-1}(T)$ *vs* T for **1** (upper) and **2** (lower). Parameters were obtained by least squares fitting a Curie-Weiss model to the data. χT *vs* T plots of the data are shown in the insets. Curie-Weiss analysis was performed in the temperature range 1.8 to 100 K.

Powder EPR Spectra

X– and Q–band powder (see experimental section for powder sample preparation) EPR spectra of **1** and **2** at room temperature are shown in Figure 4. Spectra of **1** show nearly axial symmetry ($g_{//,\perp}$= 2.239, 2.059 at X–band; $g_{1,2,3}$= 2.229, 2.049, 2.042 at Q–band) with no evidences of hyperfine structure with the copper nucleus, indicating that this interaction is collapsed by exchange.[17] EPR spectra of **2** show also axial symmetry but with $g_\perp > g_{//}$ ($g_{//,\perp}$= 2.089, 2.191, X–band; $g_{//,\perp}$= 2.085, 2.188, Q–band). Like **1**, no evidences of hyperfine structure are observed due to Cu-Cu exchange interactions. As shown below under Single Crystal EPR, this axial symmetry must not be associated with individual copper sites because EPR spectra of **2** result from the collapse of the resonances associated with two magnetically inequivalent Cu_A and Cu_B ions (Figure 2).

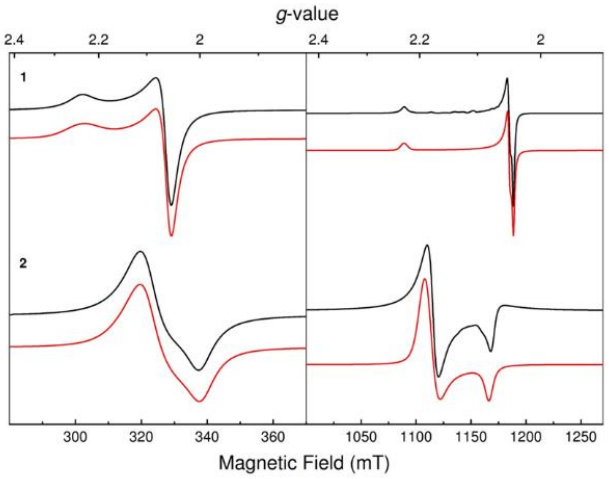

Figure 4. Powder EPR spectra (black solid lines) of **1** (upper) and **2** (lower) at room temperature together with simulation (red solid lines). Left panel, X–band; right panel, Q–band.

As said above, as no clear conclusion could be obtained from the temperature-dependent magnetic data of **1**, we performed X–band EPR measurements on powder samples as a function of temperature. Spectra taken at different temperatures (4 K-room temperature) under non-saturating conditions are essentially identical, with the most significant difference being the intensity of the EPR signal, the lower the temperature, the higher the intensity. As the power absorption of the magnetic-resonance transition is proportional to the dynamic magnetic susceptibility χ",[18] we plotted the product A*T* vs *T*, with A being the area of the EPR absorption (Figure 5). EPR results suggest a ferromagnetic behavior at high temperature, which is not observed from the magnetic measurements (Figure 3). This fact could be due to the low values of the magnetic moment at high temperature, which results in the untypical χT vs *T* curve at high temperatures.

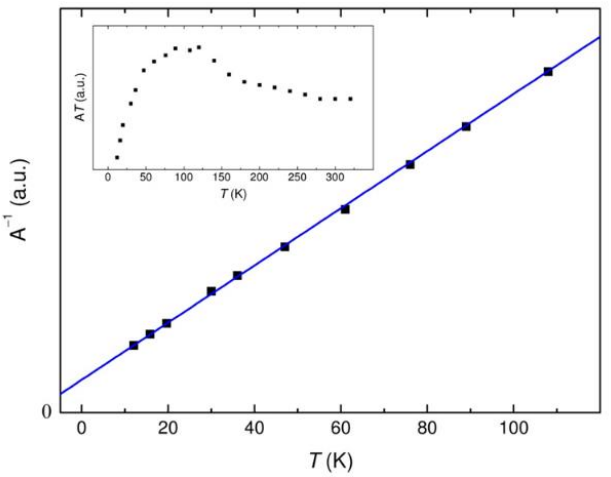

Figure 5. Inverse of the area (A) of the powder EPR absorption as a function of temperature. The inset shows the plot of A*T* vs *T*. A was obtained by double integration of the spectra.

Single Crystal EPR: the g-matrix

Single crystal EPR spectra at X– and Q–band and room temperature of **1** and **2** showed a single Lorentzian resonance line with no evidences of hyperfine structure for all tested magnetic field directions (Figures S4, S5, and S7). This indicates, in line with powder measurements, the presence of exchange interactions strong enough to collapse the hyperfine structure of the Cu(II) ions in both compounds, as well as the resonances of the two magnetically inequivalent Cu(II) ions of **2**.

For an extended lattice of magnetically equivalent *S*=1/2 spins coupled by exchange, the position of the single absorption line is given by the Zeeman Hamiltonian

$H_z = \mu_B$ **S.g.B** (1)

where $\mathbf{S} = \Sigma \mathbf{S}_i$ is the total spin, with $\mathbf{S}_i$ being the spin on the copper site *i* of the lattice (S_i=1/2), **g** is a 3×3 matrix, **B** is the external magnetic field, and μ_B is the Bohr magneton. This **g**-matrix will be referred to as the molecular **g**-matrix for **1,** as all the copper centers of the crystal lattice are magnetically equivalent. Eq 1 is also valid for **2**, but the **g**-matrix corresponds to the average of the molecular **g**-matrices of the magnetically inequivalent copper centers, $\mathbf{g} = (\mathbf{g}_A+\mathbf{g}_B)/2$; **g** which will be referred to as the crystal **g**-matrix in this case.[1a]

We determined **g**-matrix components evaluating the positions of the resonance lines by least squares fitting the derivative of a Lorentzian to the experimental spectra at X– and Q–band. The angular variations of the g^2-factors in the lab frame (Figure 6 and Figure S6) were analyzed as reported elsewhere.[19]

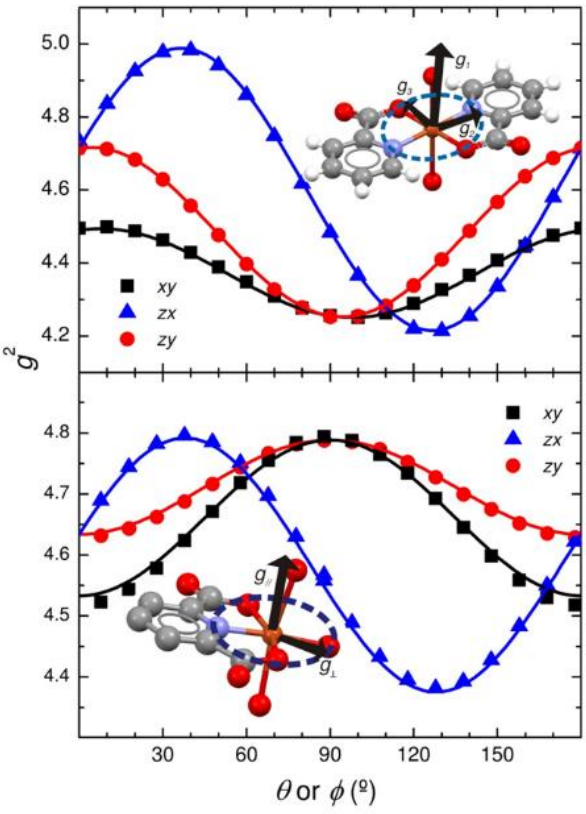

Figure 6. X–band angular variation of g^2–factors in three crystal planes of **1** (upper) and **2** (lower). The insets show the **g**-eigenvectors in the molecular frame.

g^2-matrix components for both compounds together with its eigenvalues and eigenvectors are given in Table 1. The diagonal **g**-matrix of **1** at both X– and Q–bands shows nearly axial symmetry with $g_{//}$ (**g**$_1$) ~ lying along the normal to the copper equatorial plane, and $g_{\perp}$-values lying on the equatorial plane, as expected for a copper site in a nearly square planar coordination (see inset on Figure 6 upper).

Table 1. **g**^{2}-matrix components of **1** and **2** together with eigenvalues and eigenvectors.

1	
X–Band / Q–Band	
g_{xx}^2= 4.490(1) / 4.493(2)	g_{xy}^2= 0.033(2) / 0.069(2)
g_{yy}^2= 4.256(1) / 4.218(2)	g_{zx}^2= 0.369(2) / 0.394(2)
g_{zz}^2= 4.714(1) / 4.643(2)	g_{zy}^2= –0.035(2) / –0.046(2)
g_1= 2.234(2) / 2.229(3)	**a**$_1$ = [0.595(1), 0.065(2), 0.801(1)] / [0.639(1), 0.011(3), 0.770(1)]
g_2= 2.053(2) / 2.026(3)	**a**$_2$ = [0.800(1), –0.15(4), –0.582(5)] / [0.623(5), –0.594(8), –0.509(4)]
g_3= 2.063(1) / 2.068(3)	**a**$_3$ = [0.08(3), 0.987(6), –0.14(2)] / [0.451(7), 0.804(6), –0.386(6)]
2	
X–Band / Q–Band	
g_{xx}^2= 4.533(2) / 4.479(2)	g_{xy}^2= 0.000(2) / –0.002(3)
g_{yy}^2= 4.788(2) / 4.762(2)	g_{zx}^2= 0.202(2) / 0.203(3)
g_{zz}^2= 4.634(2) / 4.613(2)	g_{zy}^2= 0.000(2) / –0.000(3)
g_1= 2.189(3) / 2.182(2)	**a**$_1$ = [0.61(7), 0.0(5), 0.79(9)] / [0.3(4), –0.9(3), 0.4(5)]
g_2= 2.092(3) / 2.081(3)	**a**$_2$ = [0.788(2), –0.000(5), –0.616(3)] / [0.811(2), 0.002(4), –0.585(3)]
g_3= 2.188(2) / 2.182(2)	**a**$_3$ = [0.0(3), –1.0(1), 0.384(4)] / [0.5(2), 0.5(6), 0.7(2)]

The **g**^{2} angular variation of **2** at X– and Q–band (Figure 6 lower and Figure S6) follows the symmetry of the monoclinic lattice of **2**, i.e. C_2 symmetry around the *b* crystal axis. This angular variation is determined by the average of the molecular *g*-factors of the magnetically inequivalent Cu_A and Cu_B ions (Figure 2A). Thus, the axial symmetry of **2** with $g_{\perp} > g_{//}$ is merely due to the particular spatial orientation of Cu_A and Cu_B sites in the crystal lattice, and must not be ascribed to the molecular **g**-matrix symmetry of single copper ions. Since copper sites of **2** present nearly square planar coordination, we calculated the molecular **g**-parameters from the crystal **g**^{2}-matrix assuming a Cu(II) site with axial symmetry.[20] The results thus obtained (Table 1) showed that the $g_{||}$ eigenvector is approximately lying along the normal to the equatorial ligand plane (see inset on Figure 6 lower), confirming our assumption. Thus, the molecular **g**-matrices in **1** and **2** indicate that the main contribution to the ground state of the copper ions is given by a $d_x2_{-y}2$ orbital in both compounds, which indicates that the unpaired spin density is mainly localized on the equatorial plane of the copper sites.

Single crystal EPR: linewidth analysis

The Hamiltonian that governs the EPR absorption spectrum of an extended system showing a single exchange-collapsed absorption is

$$H = H_z + H_{ex} + H' \quad (2)$$

where H_z was defined in eq 1, H_{ex}, H_{ex}= $-\Sigma_{i<j} J_{ij}$ $\mathbf{S}_i \cdot \mathbf{S}_j$, is the isotropic exchange interaction between the spins localized on copper sites *i* and *j* of the lattice, and H´ involves interactions such as dipole-dipole and hyperfine interactions, among others.[21]

The contributions to the EPR linewidth of the different interactions in 3D extended lattices can be rationalized on the basis of Kubo and Tomita (KT) and Anderson theories, in which H´ terms are taken as perturbations to H_z+H_{ex} (eq 2).[22] For those systems showing a single absorption line narrowed by exchange, the absorption spectra are Lorentzian with positions given by H_z (eqs 1 and 2) and a symmetrical linewidth determined by Σ M2/*J*, where M2 is the second moment of each interaction contributing to H´. This means that the resulting linewidth is a compromise between H´ terms and isotropic exchange, which yield broadening and narrowing of the resonance lines, respectively.[21, 23] The analysis of the effect of dipolar interaction on the EPR spectra under KT approach requires four time-dependent spin correlation functions usually approximated by products of the type $<S_i(t)S_j>$; < > means averages over the statistical ensemble, which involve different sites of the crystal lattice.[23] The physical meaning of these functions is how the spin state of S_i transfer its excitation to S_j as a function of time; in brief, the time decay of these functions depends on *J*, the greater the *J*, the faster the decay. The same occurs for e.g. the hyperfine interaction, but in this case, only one-site self-correlation functions are involved in the EPR linewidth contribution. Thus, the resulting Lorentzian line in 3D systems is due to the fast time decay of the time-dependent spin correlation functions of all the H´ terms, although it might not occur for systems with lower dimensionality.

The KT perturbing approach may also be used to rationalize exchange-coupled 1D systems in which dipolar interactions along the chain are predominant (also for 2D).[24] However, in this case spin correlations functions decay rapidly at short times becoming slower at larger times due to the obvious lattice constraint imposed by the 1D lattice. This determines resonance lineshapes that are in between Lorentzian and Gaussian, and W-shaped linewidth angular variations [(1-3 $\cos^2 \theta_c)^{4/3}$] with maxima for the magnetic field lying along the chain direction (θ_c= 0º) and minima at the magic angle (θ_c= 54.7º).[24] A distinct behavior should also be expected for the contribution of the hyperfine interaction between the electron spin (*S*) and its own nucleus (*I*) in a 1D system as well as for other interactions involved in H´. However, as said above, hyperfine interactions involve only one-site self-correlation functions. Since the behavior of these functions with time depends solely on the *J*-couplings between spins irrespectively of the dimensionality of the crystal lattice, their contribution to the EPR linewidth in 1D systems is similar to that observed in 3D systems. A similar situation was shown to occur for the linewidth contribution due to magnetically inequivalent centers in the lattice.[25] In summary, linewidths in 1D systems may present two distinct contributions that impact on both resonance lineshape and angular variation. When the predominant H´ term is the dipolar interaction, the resulting absorption line is in between Lorentzian and Gaussian

with W-shaped angular variation. In contrast, when interactions such as the hyperfine interaction are predominant, the lineshape should be close to Lorentzian with and angular variation similar to that of $\mathbf{g}^2$, but with the 1D W-shaped angular variation of the dipolar interaction superposed.

In line with above discussion, linewidth data shown in Figure 7 show two distinguishable main contributions. One of them is similar to that of the angular variation of $\mathbf{g}^2$ (180° periodicity), in line with angular dependences mainly governed by the second moment of the hyperfine interaction with the copper nuclei.[23, 26] The second main contribution clearly noticeable in the *xy* and *zx* planes of **1** and **2**, respectively (Figure 7) comes from dipolar interactions, which as seen above, are highly dependent on the magnetic dimensionality of the system.

To disentangle the dipole-dipole contributions from the whole linewidth angular variation, we analyzed the data in Figure 7 with the equation

$$\Delta B_{pp}(\theta,\phi) = A_1 \sin^2\theta\cos^2\phi + A_2 \sin^2\theta\sin^2\phi + A_3 \cos^2\theta + A_4\, 2\sin^2\theta\cos\phi\sin\phi + A_5\, 2\sin\theta\cos\phi\cos\theta + A_6\, 2\sin\phi\sin\theta\cos\theta + A_7 f(\theta,\phi) \quad (3)$$

in which A_1-A_6 coefficients take into account contributions with angular variations of 180° periodicity, whereas contributions from dipolar interactions are weighted by A_7. $f(\theta, \phi)$ in eq 3 represents two different alternatives to analyze the dipolar contribution, i.e. the dipolar second moment and $(1\text{-}3\cos^2\theta_c)^{4/3}$ in the 3D and 1D cases, respectively. Note also that the linewidth data in both compounds show small frequency-dependent contributions,[23, 26] which are folded into the A_1-A_6 coefficients. Least squares analysis of eq 3 to the data considering the chain model for the dipolar interaction are shown as solid lines in Figures 7; A_1-A_7 parameters are given in Table 2.

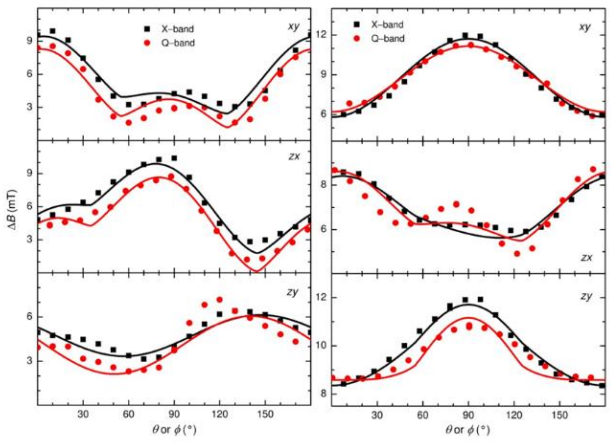

Figure 7. Angular variation of the linewidth data at X– and Q–bands (black and red) in three crystal planes of **1** (left panel) and **2** (right panel). The solid lines were obtained by least squares fitting equation 3 to the data assuming 1D magnetic behavior.

Least squares analysis to the data assuming the 3D model (second moment of the dipolar interaction) performed as explained elsewhere[27] yielded A_7-coefficients less than the uncertainty of the method (~ 0.1 mT) (not shown), which indicates that neither **1** nor **2** behave as 3D systems regarding the dipolar interaction. The good agreement between fitting and experimental data for **1** indicates a good correlation between magnetism and structure, i.e. structural and magnetic chains are the same. In contrast, least squares analyses of **2** yielded A_7 parameter, though higher, closer to the uncertainty of the EPR method (~ 0.1 mT). Although these results are also in line with a 1D magnetic behavior, the zigzag ladder chain of **2** is not clearly detected as in **1**. The 1D magnetic behavior of **1** and **2** will be rationalized in the next section.

Table 2. A_i coefficients obtained by least squares fitting eq 3 to the EPR linewidth data in Figure 7.

A_i coefficients (mT)	**1**	**2**	
X–/Q–band			
A_1	4.9/2.4	5.5/5.5	
A_2	2.4/1.4	11.4/10.4	
A_3	3.5/2.1	7.6/6.7	
A_4	0.8/0.5		
A_5	2.3/2.2	0.9/0.8	
A_6	–1.3/–1.9		
A_7		1.8/2.3	0.3/0.7

Computational calculations

1. First principle computation of the intrachain coupling *J* of **1** was performed using the coordinates from four X-ray crystal structures deposited in the CCDC, which will be identified with the respective Refcode (entry ID). Calculations indicated that the copper(II) ions are ferromagnetically coupled above ~ 50 K with *J*-values of 1.2 cm^{-1} (CUPICH02),[13o] 1.2 cm^{-1} (CUPICH17),[13s] 1.1 cm^{-1} (CUPICH14),[13g] and 0.85 cm^{-1} (CUPICH20).[13i] Although dissimilar values related to small structural differences in bonding distances of the four structures were obtained, they are indicative of the sign and magnitude of the exchange interaction transmitted by the intrachain pathway shown in Figure 1A. The interchain exchange constant computed assuming two isolated chains is within the error of the theoretical method used (J < 0.01 cm^{-1}, Figure 1). Intra and interchain *J*-values are in line with the 1D nature of **1** detected in the EPR experiment. They are also in line with EPR data above ~50 K (Figure 5), but inconsistent with the fact that **1** becomes antiferromagnetic below that temperature.

Since most crystal data show a small decrease in the length of the Cu-O_{ap} bond on lowering temperature (Figure S2), we investigated the dependence of *J* as a function of $d_{Cu\text{-}Oap}$ upon symmetrically approaching two adjacent Cu(II) complexes situated along the chain by reducing the *a*-axis of the unit cell of CUPICH17 and CUPICH20 structures (Figure 1A). These calculations showed that $d_{Cu\text{-}Oap}$ shortening yields lower ferromagnetic couplings, which becomes antiferromagnetic at distances less than 2.30 Å ($\Delta \approx 0.4$ Å) and 2.54 Å ($\Delta \approx 0.16$ Å) for CUPICH17 and CUPICH20, respectively (Figure 8).

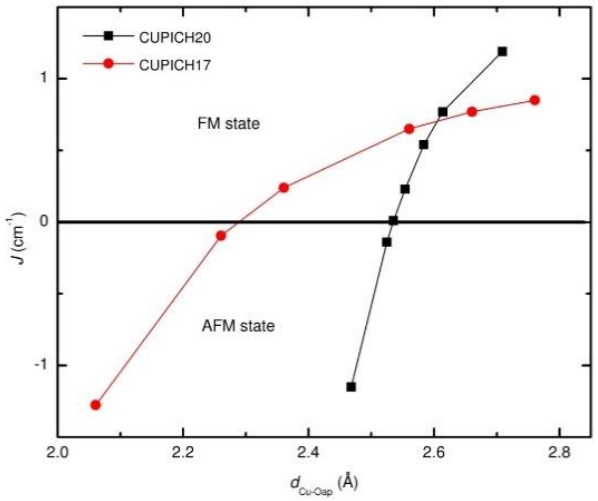

Figure 8. Exchange interaction (J) as a function of $d_{Cu\text{-}Oap}$ computed from CUPICH17 and CUPICH20 X-ray structures of **1**. The solid lines joining the symbols are to help the eye.

To rationalize the FM-AFM transition of **1**, we calculated the unpaired spin density of the Cu(II) ion and its ligands at two arbitrary distances $d_{Cu\text{-}Oap}$ of 2.706 Å (FM state) and 2.2606 Å (AFM state) using as model the CUPICH17 structure.[13s] As shown in Figure 9, a small fraction of unpaired spin density of the Cu(II) ion is delocalized on the "$p_{//}$" orbital of the apical O-carboxylate Cu(II) ligand in the ferromagnetic state, whereas on the "$p_{\perp}$" orbital in the AFM state (// and ⊥ refer to the parallel and perpendicular directions to the Cu-O_{ap} direction, respectively). Inspection of the unpaired spin density on the rest of the copper ligands indicated that it does not significantly change as a function of $d_{Cu\text{-}Oap}$. Thus, the computational results would indicate that the cause of the FM-AFM change implies the reorganization of the small unpaired copper spin delocalization on the Cu(II) apical ligand.

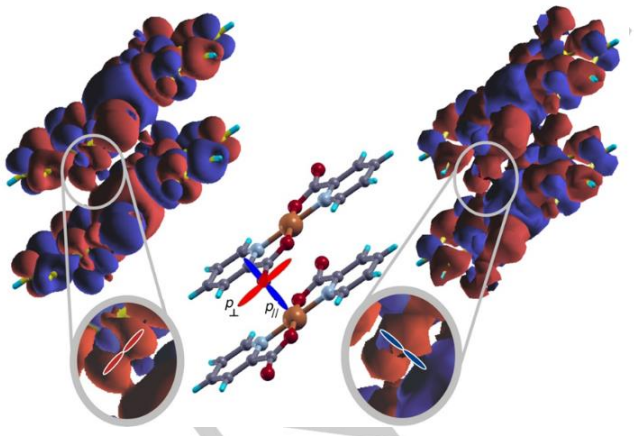

Figure 9. Unpaired spin density of the AFM (left) and FM (right) states. Alfa and beta spin densities are in blue and red, respectively. The scheme at the center displays the 2p-type orbitals of the O_{ap} ligand, where // and ⊥ symbols refer to the parallel and perpendicular directions to the Cu-O_{ap} direction, respectively. The figure was constructed with an isosurface value of 0.0001 e/Å3.

2. Figure 10 shows a schematic view of the ladder-type chains of **2** depicted in Figure 2, which is also named triangle-type ladder in the literature.[28] Calculations of the inter-chain exchange interactions (J_4, see also Figure 2B) as explained in the experimental section yielded values within the error of the method (J ~ 0.01 cm^{-1}), and hence not considered in our analysis.

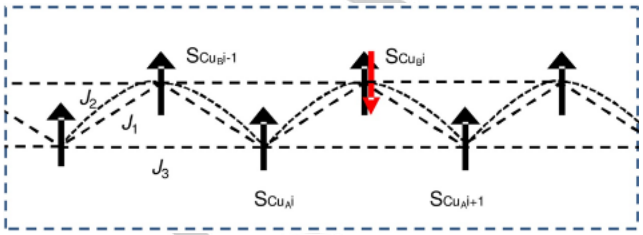

Figure 10. Schematic view of the zigzag ladder chain of **2** indicating the isotropic exchange constants associated with the pathways linking neighboring spins. J_1 and J_2 correspond to the exchange interactions transmitted through the rungs where J_3 along the rails (see also Figure 2A). The ferromagnetic state of the supercell is indicated with black arrows (spins up), whereas the arrow in red indicates a spin flipped down.

The exchange Hamiltonian for these types of systems can be written

$H = -(J_1+J_2)\, S_{CuBi}.(\mathbf{S}_{CuAi}+\mathbf{S}_{CuAi+1}) - J_3\,(\mathbf{S}_{CuAi}.\mathbf{S}_{CuAi+1}+\mathbf{S}_{CuBi}.\mathbf{S}_{CuBi+1})$ (4)

in which the sum over the index i is omitted for simplicity. Computing of the energy of the periodic 6 Cu-containing chain (Figure 10) with all spins up (↑↑↑↑↑↑ state), and with one spin down (indicated in red in Figure 10, ↑↑↑↓↑↑ state), yielded, $\Delta E_{AFM\text{-}FM}$ = 7 cm^{-1}, which is in line with the ferromagnetic nature of **2** revealed by magnetic susceptibility data (lower panel of Figure 3). By applying the Hamiltonian in equation 4 to the spin states depicted in Figure 10, we obtained $H|\uparrow\uparrow\uparrow\uparrow\uparrow\uparrow> = -3/2\,(J_1 + J_2 + J_3)$ and $H|\uparrow\uparrow\downarrow\uparrow\uparrow\uparrow> = -\tfrac{1}{2}\,(J_1 + J_2 + J_3)$. Then $\Delta E_{AFM\text{-}FM} = (J_1 + J_2 + J_3)$ = 7 cm^{-1}, which comprises contributions from J_1, J_2 and J_3.

In order to elucidate the contribution in both sign and magnitude of J_1, J_2 and J_3 to J, we systematically rotated the water molecules O_{5w} and O_{6w} together or individually to weaken the H-bond interaction associated with J_2 and J_3 pathways (Figure 2A). Rotating of the six O_{5w} water molecules involved in the J_2 pathway (J_1 and J_3 pathways remained unmodified) yielded a destabilization of both the FM and AFM states, but the resulting ground state remained ferromagnetic ($\Delta E_{AFM\text{-}FM}=(J_1 + J_3)$= 5.4 cm^{-1}). This showed that J_2 stabilizes the ferromagnetic state. The same result was obtained by rotating the six O_{6w} water molecules (J_1 and J_2 pathways remained unmodified) which yielded $\Delta E_{FM\text{-}AFM}(O6w) =(J_1 + J_2)$ = 6.7 cm^{-1}. Rotating of both O_{5w} and O_{6w} (J_1 pathway remained unmodified) yielded $\Delta E_{AFM\text{-}FM}(O_{5w}/O_{6w}) = J_1$ = 6.1 cm^{-1}. These procedures altogether indicated that the three chemical pathways transmit ferromagnetic exchange interactions.

Conclusion

The magnetic properties of two complexes containing single and zigzag ladder Cu(II) ion chains have been characterized and analyzed on the basis of theoretical grounds. Single crystal EPR spectroscopy in conjunction with magnetic susceptibility measurements confirmed that both compounds present magnetic chains in which the copper ions are weakly coupled by isotropic exchange. EPR measurements as a function of temperature **1** suggested that the copper ions are ferromagnetically coupled at temperatures above 50 K but antiferromagnetically below that temperature. Computational calculations indicated that this FM→AFM change is due to $d_{Cu\text{-}Oap}$ shortening on lowering temperature, which reorganizes the small Cu(II) unpaired spin density delocalized onto the O_{ap}-ligand to copper. Single crystal EPR spectroscopy experiments at very low temperature are necessary to verify whether the room-temperature 1D magnetic behavior is kept in the AFM state.

Although the zigzag ladder chain of **2** can be classified as a 1D magnetic lattice, single crystal EPR indicated a 1D magnetic behavior less evident than that of **1**. Magnetic susceptibility measurements in conjunction with computational calculations showed that the pathways that give rise to the 1D ladder transmit ferromagnetic exchange interactions, with the larger exchange interaction transmitted through the rungs. However, it is evident that the weaker exchange interactions transmitted along the rails have some influence on the spin dynamic of **2**, which results in a magnetic behavior with some differences relative to that of single magnetic chains.

Experimental Section

Materials: All chemicals, of commercially available reagent grade, were used as received. Synthesis of **1** and **2** were performed as reported elsewhere but with some modifications.[13r, 14c]

1: $Cu(CH_3COO).H_2O$ (0.5 mmol, 0.099 g, Fluka) and picolinic acid (1 mmol, 0.123 g, Sigma-Aldrich) were dissolved in 100 mL of water. The mixture was stirred at 80 °C until dissolution. The solution was filtered with a 0.22 μm Millipore cellulose nitrate membrane and left to evaporate slowly at room temperature. After a few days blue-colored prismatic single crystals were obtained, which were filtered, washed with a small amount of cold water, and air dried.

2: $CuCO_3.Cu(OH)_2$ (4 mmol, 0.221 g, Fluka) was dissolved together with dipicolinic acid (4 mmol, 0.167 g, Sigma) in 200 mL of water. The solution was stirred for two hours at 60°C, filtered with a 0.22 μm Millipore cellulose nitrate membrane and then left to evaporate at 60°C. After a few days light blue-colored prismatic single crystals were obtained, filtered, rinsed with cold water, and air dried.

Structure and Morphology of single crystals: Powder X-ray diffraction measurements were performed on a Shimadzu XD-D1 diffractometer to confirm that the structures correspond to those previously reported (see Results section). The morphology of the single crystals, necessary to orient the sample for the EPR experiment, were determined on a Carl Zeiss Axiolab goniometric microscope. Powder samples either for EPR spectroscopy or magnetic measurements were prepared by grinding single crystal samples with well-defined morphology.

EPR Measurements: X- and Q-band CW-EPR spectra were performed on a Bruker EMX-Plus spectrometer equipped either with a nitrogen continuous-flow cryostat (100-340 K) or with an Oxford helium continuous-flow cryostat (4-100 K) and a rectangular cavity and 100 kHz field modulation.

Single crystals of **1** and **2** were oriented by gluing their (011) and (100) faces, respectively, to a cleaved KCl cubic holder which defined a set of orthogonal *xyz* laboratory axes. The *x* axis corresponds to the crystal *a* axis of **1**, whereas $y = b\times[\sin(90\text{-}\gamma), \cos(90\text{-}\gamma), 0]$ and $z = c\times[\sin\theta\cos\phi, \sin\theta\sin\phi, \cos\theta]$. For **2**, *y* and *z* axes correspond to the crystal *b* and *c* axes, respectively. Sample holders were positioned at the center of the microwave cavity as explained elsewhere,[19] and rotated at 10° intervals with the magnetic field in the *xy*, *zx* and *zy* planes. EPR spectra were analyzed with the EasySpin toolbox [29] and homemade programs based on MATLAB®.

Magnetic Measurements: Magnetic susceptibility measurements were obtained with a Quantum Design MPMS2 SQUID magnetometer. Measurements were performed on powder samples of **1** (53.0 mg) and **2** (40.7 mg) using a gelatin capsule as sample holder with a small (and known) diamagnetic contribution at 50 mT in the temperature range of 1.8 and 300 K. The contribution of the gelatin capsule was subtracted from the measured values. The molar magnetic susceptibility values were corrected for diamagnetism using the Pascal's constants (χ_{DIA} = -126.0×10^{-6} $cm^3\ mol^{-1}$ and -93.9×10^{-6} $cm^3\ mol^{-1}$ for **1** and **2**, respectively).[16]

Computational Calculations: Isotropic exchange interactions were calculated using periodic boundary conditions with the first–principle screened exchange hybrid density functional of Heyd, Scuseria, and Ernzerhof (HSE)[30] and the basis set 6–311G(d,p). Both compounds were modeled assuming periodic short chains of Cu(II) centers within the unit cell, two for **1**, and six for **2**. The isotropic exchange coupling constant was computed with the equation $J = (E_{AFM} - E_{FM})$, where E_{FM} is the energy of a ferromagnetically coupled chain, and E_{AFM} is the energy of the same chain but with one flipped spin. Computed isotropic exchange constants comprise both covalent and non-covalent interactions. Inter-chain exchange constants were computed assuming two adjacent chains with two copper centers each. In the case of **2**, to evaluate the different exchange constants contributing to *J*, the water molecules O_{5w} and O_{6w} were rotated and then FM and AFM energies were computed. Calculations were performed with the structural data of both compounds without relaxation.[13g, 13i, 13o, 13s]

Acknowledgements

We thank FONCyT, CONICET, and CAI+D-UNL for financial support. A.L.P. thanks CONICET for a fellowship grant. S. D. and C.D.B. are members of CONICET-Argentina. Computations were performed in the cluster *Pirayu* acquired with funding from ASACTEI, Government of Santa Fe.

Keywords: Copper. EPR. Exchange interaction. Magnetic chain. One dimension system.

References

[1] a) A. C. Rizzi, N. I. Neuman, P. J. González, C. D. Brondino, *Eur. J. Inorg. Chem.* **2016**, 192-207; b) L. Bogani, A. Vindigni, R. Sessoli, D. Gatteschi, *J. Mater. Chem.* **2008**, *18*, 4750-4758.

[2] Y. Journaux, J. Ferrando-Soria, E. Pardo, R. Ruiz-Garcia, M. Julve, F. Lloret, J. Cano, Y. Li, L. Lisnard, P. Yu, H. Stumpf, C. L. M. Pereira, *Eur. J. Inorg. Chem.* **2018**, *2018*, 228-247.

[3] C. C. Moser, J. L. R. Anderson, P. L. Dutton, *Biochim. Biophys. Acta, Bioenerg.* **2010**, *1797*, 1573-1586.

[4] M. G. Rivas, P. J. González, F. M. Ferroni, A. C. Rizzi, C. D. Brondino, *Sci. Rev. Few.* **2020**, *1*, 6-23.
[5] R. Calvo, E. C. Abresch, R. Bittl, G. Feher, W. Hofbauer, R. A. Isaacson, W. Lubitz, M. Y. Okamura, M. L. Paddock, *J. Am. Chem. Soc.* **2000**, *122*, 7327-7341.
[6] a) J. Ferrando-Soria, J. Vallejo, M. Castellano, J. Martínez-Lillo, E. Pardo, J. Cano, I. Castro, F. Lloret, R. Ruiz-García, M. Julve, *Coord. Chem. Rev.* **2017**, *339*, 17-103; b) E. Coronado, *Nat. Rev. Mater.* **2020**, *5*, 87-104; c) S. Prabhulkar, H. Tian, X. Wang, J.-J. Zhu, C.-Z. Li, *Antioxid. Redox Signaling.* **2012**, *17*, 1796-1822; d) M. Cortijo, V. Bulicanu, K. S. Pedersen, M. Rouzières, J. Bendix, R. Clérac, E. A. Hillard, *Eur. J. Inorg. Chem.* **2018**, *2018*, 320-325; e) C. Coulon, H. Miyasaka, R. Clérac, in *Single-Molecule Magnets and Related Phenomena* (Ed.: R. Winpenny), Springer Berlin Heidelberg, Berlin, Heidelberg, **2006**, pp. 163-206; f) Z.-X. Li, Y.-F. Zeng, H. Ma, X.-H. Bu, *Chem. Commun.* **2010**, *46*, 8540-8542; g) M.-G. Alexandru, D. Visinescu, S. Shova, M. Andruh, F. Lloret, M. Julve, *Eur. J. Inorg. Chem.* **2018**, *2018*, 360-369; h) E. Q. Gao, S. Q. Bai, C. F. Wang, Y. F. Yue, C. H. Yan, *Inorg. Chem.* **2003**, *42*, 8456-8464.
[7] T. Ezuhara, K. Endo, K. Matsuda, Y. Aoyama, *New J. Chem.* **2000**, *24*, 609-613.
[8] R. E. Dietz, F. R. Merritt, R. Dingle, D. Hone, B. G. Silbernagel, P. M. Richards, *Phys. Rev. Lett.* **1971**, *26*, 1186-1188.
[9] a) I. Y. Drozdyuk, K. Y. Maryunina, R. Z. Sagdeev, V. I. Ovcharenko, E. G. Bagryanskaya, M. V. Fedin, *Mol. Phys.* **2013**, *111*, 2903-2907; b) R. A. Allao, A. K. Jordao, J. A. L. C. Resende, A. C. Cunha, V. F. Ferreira, M. A. Novak, C. Sangregorio, L. Sorace, M. G. F. Vaz, *Dalton T.* **2011**, *40*, 10843-10850.
[10] a) L. J. de Jongh, A. R. Miedema, *Adv. Phys.* **1974**, *23*, 1-260; b) S. J. Blundell, F. L. Pratt, *J. Phys: Condens. Matter.* **2004**, *16*, R771-R828.
[11] a) M. V. Fedin, S. L. Veber, K. Y. Maryunina, G. V. Romanenko, E. A. Suturina, N. P. Gritsan, R. Z. Sagdeev, V. I. Ovcharenko, E. G. Bagryanskaya, *J. Am. Chem. Soc.* **2010**, *132*, 13886-13891; b) S. L. Veber, M. V. Fedin, A. I. Potapov, K. Y. Maryunina, G. V. Romanenko, R. Z. Sagdeev, V. I. Ovcharenko, D. Goldfarb, E. G. Bagryanskaya, *J. Am. Chem. Soc.* **2008**, *130*, 2444-2445.
[12] A. L. Pérez, N. I. Neuman, R. Baggio, C. A. Ramos, S. D. Dalosto, A. C. Rizzi, C. D. Brondino, *Polyhedron.* **2017**, *123*, 404-410.
[13] a) R. Cargnelutti, C. P. Delgado, R. Cervo, B. Tirloni, R. A. Burrow, E. S. Lang, *New J. Chem.* **2018**, *42*, 17185-17189; b) D. M. Čechová, Jan *CSD Commun.* **2020**; c) Y.-M. X. Chen, Qing-Fan; Xian, Jing-Chun, *Chinese J. Spectroscopy Lab.* **2004**, *21*, 167; d) W. H. Clegg, R.W. , *CSD Commun.* **2017**; e) D. K. Das, V. K. Kumar Pampana, K. C. Hwang, *Chem. Sci.* **2018**, *9*, 7318-7326; f) M. Du, X.-H. Bu, M. Shionoya, M. Shiro, *J Mol Struct.* **2002**, *607*, 155-161; g) D. Dutta, A. D. Jana, A. Ray, J. Marek, M. Ali, *Indian J. Chem., Sect. A.* **2008**, *47*, 1656-1660; h) E. C. C. Lingafelter, H.J. , *ACA Abstr. Papers (Winter).* **1970**, *25*; i) L. L. Liu Zheng, Li Wei, Chen Shiliang, *J. Mol. Sci.* **2014**, *30*, 106-111; j) J. H. Luo, M. C. Hong, Q. Shi, Y. C. Liang, Y. J. Zhao, R. H. Wang, R. Cao, J. B. Weng, *Transition Met. Chem.* **2002**, *27*, 311-315; k) M. Mikuriya, H. Azuma, R. Nukada, Y. Sayama, K. Tanaka, J.-W. Lim, M. Handa, *Bull. Chem. Soc. Jpn.* **2000**, *73*, 2493-2498; l) R. N. S. Patel, Yogendra Pratap; Singh, Yogendra; Butcher, Raymond J., *CSD Commun.* **2015**; m) F. A. A. G. Paz, P.I.; Nogueira, H.I.S.; Trindade, T.; Klinowski, J., *Private Commun.* **2003**; n) J. Ran, X. Li, Q. Zhao, Z. Qu, H. Li, Y. Shi, G. Chen, *Inorg. Chem. Commun.* **2010**, *13*, 526-528; o) P. Segl'a, M. Jamnický, M. Koman, J. Šima, T. Glowiak, *Polyhedron.* **1998**, *17*, 4525-4533; p) Z. A. Siddiqi, P. K. Sharma, M. Shahid, M. Khalid, Anjuli, A. Siddique, S. Kumar, *Eur. J. Med. Chem.* **2012**, *57*, 102-111; q) K. A. Siddiqui, *J. Coord. Chem.* **2012**, *65*, 4168-4176; r) A. Takenaka, A. Furusaki, I. Nitta, H. Utsumoi, T. Yamamoto, *Nippon kagaku zassi.* **1970**, *91*, 928-935; s) J. Tessarolo, A. Venzo, G. Bottaro, L. Armelao, M. Rancan, *Eur. J. Inorg. Chem.* **2017**, *2017*, 30-34; t) L.-j. S. Wang, Li-ping; Liu, Chun, *J. Northeast Normal Univ. Nat. Sci. Ed.* **2006**, *38*, 138; u) Q. Wang, Z. Yu, Q. Wang, W. Li, F. Gao, S. Li, *Inorg. Chim. Acta.* **2012**, *383*, 230-234; v) J. Xia, M. Zhang, B. Zhao, P. Cheng, *Chin. J. Inorg. Chem.* **2006**, *22*, 1406-1410; w) Q. H. Zhao, M. S. Zhang, R. B. Fang, *J. Struct. Chem.* **2006**, *47*, 764-767; x) L. L. Zheng, Lai; Wei, Li; Shiliang,Chen, *J. Molec. Sci.* **2014**, *30*, 106.
[14] a) P. M. Masárová, Jan, *CSD Commun.* **2020**; b) C. Xie, Z. Zhang, X. Wang, X. Liu, G. Shen, R. Wang, D. Shen, *J. Coord. Chem.* **2004**, *57*, 1173-1178; c) M. B. Cingi, A. C. Villa, C. Guastini, M. Nardelli, *Gazz. Chim. Ital.* **1971**, *101*, 825; d) Y.-m. S. Han, Shi-lin; Zhang, Huai-min; Song, Shuang; Wu, Lan-zhi; Yang, Li-rong, *Huaxue Yanjiu.* **2012**, *23*, 82.
[15] a) C. Janiak, *Dalton Trans.* **2003**, 2781-2804; b) R. Shrivastava, R. Nagar, G. Ravishankar, R. Upreti, U. Chaturvedi, *Indian J. Med. Res.* **2007**, *126*, 440-446; c) Ö. Tamer, B. Sarıboğa, İ. Uçar, O. Büyükgüngör, *Spectrochim. Acta, Part A.* **2011**, *84*, 168-177; d) M. Pilar Brandi-Blanco, J. María González-Pérez, D. Choquesillo-Lazarte, R. Carballo, A. Castiñeiras, J. Niclós-Gutiérrez, *Inorg. Chem. Commun.* **2003**, *6*, 270-273.
[16] O. Kahn, *Molecular Magnetism*, VCH Publishers New York, **1993**.
[17] a) C. D. Brondino, R. Calvo, A. M. Atria, E. Spodine, O. R. Nascimento, O. Peña, *Inorg. Chem.* **1997**, *36*, 3183-3189; b) N. I. Neuman, V. G. Franco, F. M. Ferroni, R. Baggio, M. C. G. Passeggi, A. C. Rizzi, C. D. Brondino, *J. Phys. Chem. A.* **2012**, *116*, 12314-12320.
[18] J. A. Weil, J. R. Bolton, *Electron Paramagnetic Resonance: Elementary Theory and Practical Applications*, 2nd ed., John Wiley & Sons, Hoboken, New Jersey, **2007**.
[19] J. M. Schveigkardt, A. C. Rizzi, O. E. Piro, E. E. Castellano, R. Costa de Santana, R. Calvo, C. D. Brondino, *Eur. J. Inorg. Chem.* **2002**, 2913-2919.
[20] R. Calvo, M. A. Mesa, *Phys. Rev. B.* **1983**, *28*, 1244-1248.
[21] a) R. Calvo, *Appl. Magn. Reson.* **2007**, *31*, 271-299; b) S. K. Hoffmann, W. Hilczer, J. Goslar, *Appl. Magn. Reson.* **1994**, *7*, 289-321.
[22] a) R. Kubo, K. Tomita, *J. Phys. Soc. Jpn.* **1954**, *9*, 888-919; b) P. W. Anderson, P. R. Weiss, *Rev. Mod. Phys.* **1953**, *25*, 269-276.
[23] Z. G. Soos, T. Z. Huang, J. S. Valentine, R. C. Hughes, *Phys. Rev. B.* **1973**, *8*, 993-1002.
[24] P. M. Richards, *Magnetic Resonance in One- and Two-Dimensional Systems in Local properties at phase transitions*, North-Holland Pub. Co., Amsterdam; New York, **1976**.
[25] a) C. D. Brondino, N. M. C. Casado, M. C. G. Passeggi, R. Calvo, *Inorg. Chem.* **1993**, *32*, 2078-2084; b) A. C. Rizzi, O. E. Piro, E. E. Castellano, O. R. Nascimento, C. D. Brondino, *Inorg. Chim. Acta.* **2000**, *305*, 19-25.
[26] A. M. Gennaro, R. Calvo, *J. Phys: Condens. Matter.* **1990**, *2*, 2873-2873.
[27] A. L. Pérez, A. Kemmerer, M. A. Rey, S. D. Dalosto, C. A. Ramos, M. C. G. Passeggi, A. C. Rizzi, C. D. Brondino, *Eur. J. Inorg. Chem.* **2018**, *2018*, 4604-4613.
[28] Y. I. Dublenych, *Phys. Rev. B.* **2016**, *93*, 054415.
[29] S. Stoll, A. Schweiger, *J. Magn. Reson.* **2006**, *178*, 42-55.
[30] J. Heyd, G. E. Scuseria, M. Ernzerhof, *J Chem Phys.* **2003**, *118*, 8207-8215.

Entry for the Table of Contents

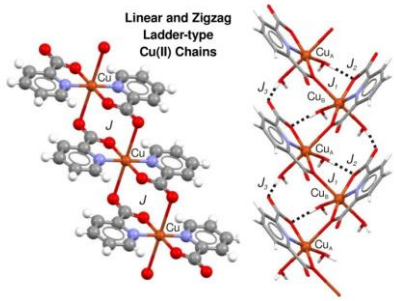

The picture shows two copper complexes with picolinic and dipicolinic acids containing single and zigzag ladder structural Cu(II) ion chains. Magnetic measurements, single crystal EPR, and computational calculations are used to unveil the magnetic dimensionality of both systems. Experimental and theoretical results confirmed that the structural chains in both compounds behave as magnetic chains despite copper ions are weakly coupled by isotropic exchange.